Development Of A Portable EOG Device For Signal Acquisition And Movement Characterization

Luis C. Parra.[a,*], Andrés F. Rodriguez.[a], Diego Paéz.[a] and Diana Martínez.[a]

***Abstract*—Bioelectrical signals produced by saccadic movement are widely studied in biomedical applications like dream cycles, polysomnography, and motor disabilities among others. In this study, the development of a portable electrooculograph (EOG) device is presented. The signal acquisition, hardware, and software modules are integrated into a board prototype. An Analog Front End microchip, Analog to digital converter, and ESP32-WROOM-32D SOC have been used for this purpose. The digitized EOG signal is transmitted to a PC using Bluetooth as the wireless communication protocol. It can also be transmitted using the UART protocol as the wired communication protocol, requiring a USB converter device. EOG signals are provided by horizontal and vertical ocular movements. Noisy performance is reduced by the digital filter design. Simulation and testing evaluated the selected digital filter. The accomplishment of the presented prototype was authenticated through its implementation with two subjects, where a correct visualization of the measured EOG signals is presented, even when the 60 Hz noise is mixed with the ocular signals. At the same time, the characterization of the signal was established.**

***Index Terms*—EOG signals, analog filter, digital filter, characterization data, Wavelet transform.**

I. Introduction

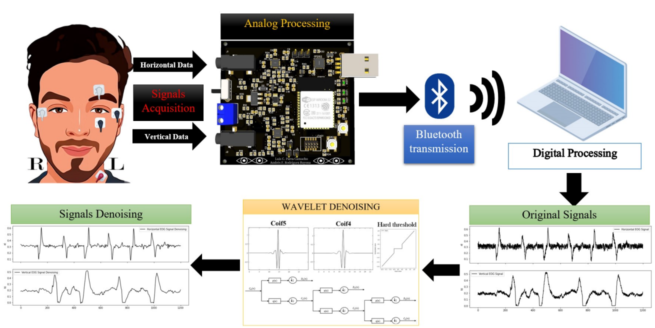

Fig. 1. EOG signal acquisition and processing.

The World Health Organization (WHO) and Pan American Health Organization (PAHO) reports that more than one billion people are under some type of disability [1] [2], which corresponds to approximately 15 percent of the world population, where up to 190 million people (3.8 %) are 15 years or older who have difficulty functioning easily and often require health services. Nowadays, the growing trend of health devices allows the emergence of new opportunities for this population. According to the 25 articles of the United Nations Convention on the Rights of Persons with Disabilities, an attempt is made to achieve the highest health standards without discrimination, and technology and science advances can offer alternatives to this population to improve their life quality by tools or applications, providing them with the ability to perform tasks that would be limited due to their disabilities. [1] [3]

Eye movement reading is possible due to the change in corneal-retinal potential. The retina has a resting bio-electric potential, which is electronegative concerning the cornea. In this way, the turns of the eyeball cause changes in the direction of the vector corresponding to this electric dipole, thus, the eye movement generates a small voltage between the cornea and the retina [4]. The method to acquire this signal based on the recording of the potential difference between the cornea and the retina is called an electrooculogram. These signals are obtained through electrodes that are distributed at strategic points close to the eyes [5]. Nowadays, there are several applications of EOG such as devices based on EOG signals that offer help to people with some type of motor disability, to control wheelchairs, a mouse or keyboard [6]; it also allows the detection of diseases such as Best's disease and Stargardt's disease as well as diseases related to sleep disturbance such as narcolepsy, REM sleep behavior disorder. [7]

The objective of this study is to prototype a portable electrooculograph device that allows acquiring the waveform signal consequential to the eye movement both vertical and horizontal, letting long-term communication to a PC through the Bluetooth technology while maintaining signal quality. The design process of the presented prototype starts from the acquisition of data through electrodes established in the specific horizontal and vertical positions defined. An analogical band-pass filter between 0-50 Hz was designed by integration of a low pass filter and two poles high pass filter using an Analog Front End (AFE) device AD8232 microchips. Besides, the designed device transmits the data to an Open-source software on a PC through wireless communication using Bluetooth technology assuring the required Nyquist frequency for this purpose, and then it is digitally filtered by the wavelet transform method and presented graphically. The use of wavelet transform allows presenting a signal with a lower noise component and with no lack of information. The digital process was evaluated in different wavelet forms and statisticians parameters obtaining the best method for each movement channel. A printed circuit board (PCB) was developed for this purpose and its design, configuration, and results are presented.

[a]Mechatronic Engineering Faculty, Santo Tomas University, Bucaramanga, Colombia. luiscarlos_2214@hotmail.com; andresfer1105@gmail.com; diego.paez@ustabuca.edu.co; diana.martinez@ustabuca.edu.co

II. Material and Methods

A. EOG signal acquisition

Capturing eye signals may be performed by various methods, which let a digital representation. In this study, infrared oculography, Purkinje images tracking, video-oculography and electrooculography were analyzed according to their advantages and disadvantages, where electrooculography is the chosen method, because of its capability to read movements such as the saccade and blinks, requiring only the superficial connection of the electrodes to the patient's skin, being able to record angles of up to 70° [8] [9]. The reference electrodes used in this study to obtain the corneum-retinal potential are the non-invasive and low-cost gel electrodes 3M 2228. Figure 2 explains the distribution of electrodes.

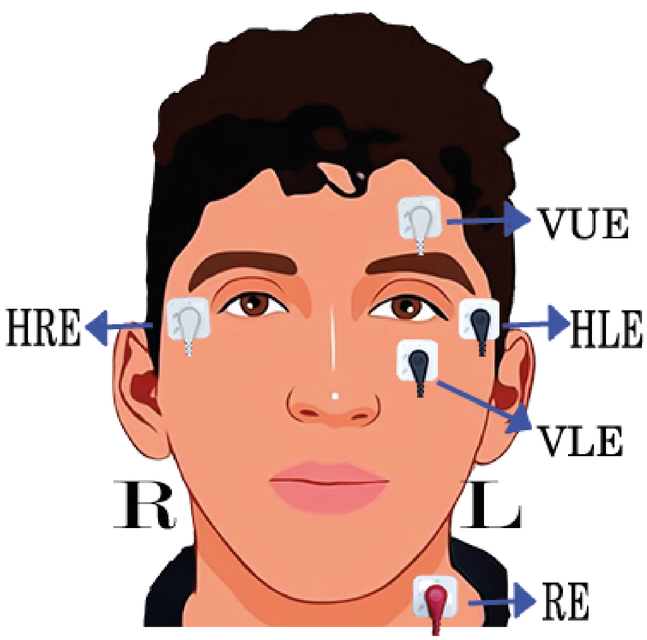

Fig. 2. Electrodes distribution. HLE: Horizontal Left Electrode. HRE: Horizontal Right Electrode. VUE: Vertical Upper Electrode. VLE: Vertical Lower Electrode. RE: Reference Electrode. R: Right side. L: Left side.

The designed hardware is represented in the Figure 3. This system was built principal around the Analog Front End (AFE), which the aim of obtaining the signal and establish a correct EOG signal processing. At the same time, the exposed diagram contains a classification by colors according to their operation. The prototype includes two acquisition systems:

- Horizontal EOG AFE: It's main function is to process analogically the right and left signals.
- Vertical EOG AFE: It's main function is to process analogically the up and down signals.

Furthermore, the AFE devices share the reference electrode as is presented in Figure 3. Besides, the device lets two different communications protocols as is presented:

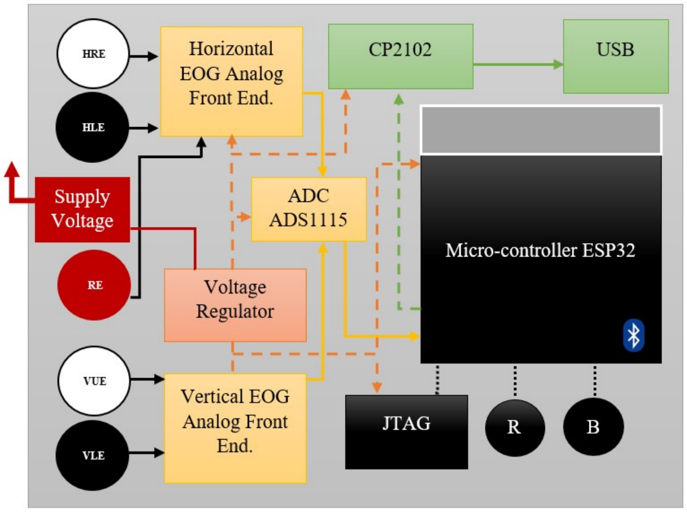

Fig. 3. Conceptual Schematic Of The EOG prototype. HRE: Horizontal Right Electrode. HLE: Horizontal Left Electrode. VUE: Vertical Upper Electrode. VLE: Vertical Lower Electrode. EOG: Electrooculography. CP2102: UART to USB converter, ADC: Analog to digital converter. JTAG: Joint Test Action Group. R: Reset button. B: Bootload button. Furthermore, the important stages are represented by colors. Red: Voltage supply prototype. Yellow: EOG signal acquired. Black: SOC set up. Green: USB protocol.

- Serial: The CP2102 device lets the prototype the conversion from UART to Serial protocol in benefit of the transmission and reception of information.
- Bluetooth: The ESP32-WROOM-32D SOC has an embedded Bluetooth module, allowing for prototype portability.

Besides those sensing and communication subsystems, the presented instrument also includes:

- Power supply subsystem through batteries.
- Power supply subsystem through USB connector.
- Voltage regulator subsystem managing the system battery.
- JTAG (Joint Test Action Group) interface for system programming and debugging.
- Bootload Button for system program and debugging by the serial interface.
- Reset Button managing the loaded program in ESP32-WROOM-32D SOC.

B. Analog filter design

The AD8232 microchip implementation reduces the interference signals. An AFE integrated circuit allows the acquisition and conditioning of biological signals according to the operating frequencies. A. López Martínez established a range of frequencies between 0-50 Hz to the EOG signals, according to a study by J.Enderle. Nevertheless, other studies reveal that the totality useful of its spectrum lies down 38 Hz. [10]

To obtain an EOG signal with useful information in the operating frequency required, the AD8232 was configured with a bandpass filter composed by 0.5 Hz two-pole high-pass filter and a 40 Hz two-pole low-pass filter, used in other

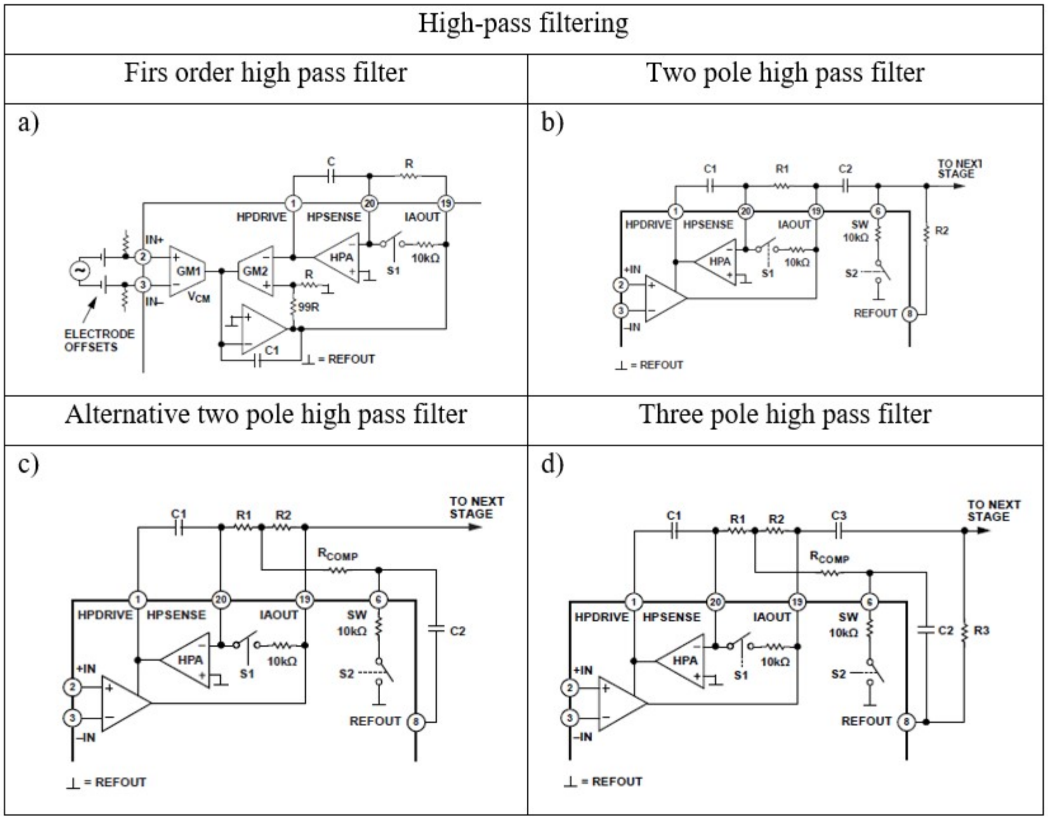

Fig. 4. High-pass filter settings. Characteristics: a). High offset rejection. b) Better frequency rejection. Increased signal distortion. c). Low output impedance d). best settling time response. Instrumentation Amplifier Positive Input. -IN: Instrumentation Amplifier Negative Input. High signal gain ($G = 100$). The image was modified from [11], Copyright © 2019, Analog Devices, Inc.All Rights Reserved.

applications as cardiac monitor configuration explained in the AD823X chip's documentation [11].

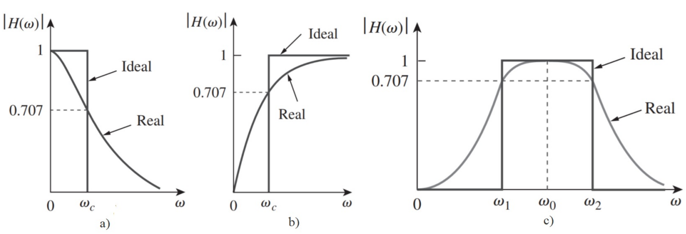

Fig. 5. Filters settings. a) Low-pass filter b) High-pass filter c) Band-pass filter.The image was modified from [12], Copyright © 2013, 2006, regarding the third edition in Spanish by McGRAW-HILL/INTERAMERICANA EDITORES, S.A. de C.V, Inc.All Rights Reserved.

1) High-Pass Filter: The AD8232 microchip is a very versatile device that allows high-pass filters from first to third order. Figure 5 shows the behavior of the different filters and Figure 4 shows the different analog filter settings provided by the AD8232 microchip. For the high-pass filter, the setting used in this study is the alternative two-pole due to its low output impedance as shown in figure 4 and table I.

TABLE I
HIGH-PASS FILTERING CHARACTERISTICS.

N°	Filter Order	L.F Rejection [1]	Signals Distortion	Output Z [2]
1	1	Good	Low	Low
2	2	Better	Medium	Higher
3	2	Good	Medium	Low
4	3	Best	Highest	Higher

Equation (1) corresponds to the cutoff frequency of the high-pass filter for the circuit configuration of the Figure (6).

$$F_H = \frac{10}{2\pi\sqrt{R_1 C_1 R_2 C_2}} \quad (1)$$

Using the values $R_1 = R_2 = 10M\Omega$ and $C_1 = C_2 = 330nF$, corresponding to AD8232 chip's documentation (Figure 6), the cutoff frequency of the high-pass filter is 0.48 Hz. The high-pass filter gain is $G_H = 100$, according to the Instrumental Amplifier (INA) provide by the AD8232 microchip.

[1] Low frequency rejection response according to filter order. [11]

[2] Refers to the drive capability of the high-pass filter. Low output impedance is desirable to allow flexibility in the selection of values for a low pass filter. [11]

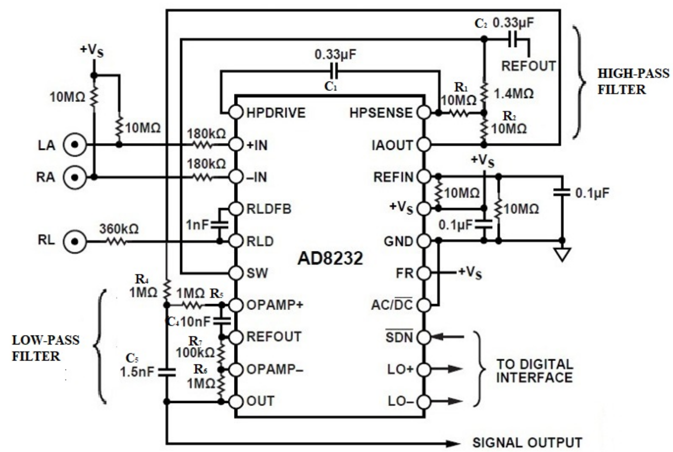

Fig. 6. AD8232 Analog Filtering Setting. RL: Reference electrode. IN: Electrodes inputs. Vs: Voltage Supply. LO: Lead-off detection inputs. The image was modified from [11], Copyright © 2019, Analog Devices, Inc.All Rights Reserved.

2) Low-Pass Filter: For EOG signals the low pass filter must operate in a cut frequency over 40 Hz. Equation (2) correspond to the cut-off frequency of the low-pass filter and figure (5). a) shows the behavior of the low-pass filter according to the cut-off frequency for the circuit configuration of Figure (6).

$$F_L = \frac{1}{2\pi\sqrt{R_4 C_4 R_5 C_5}} \tag{2}$$

Using the values $R_4 = R_5 = 1M\Omega$, $C_5 = 1.5nF$, and $C_4 = 10nF$, corresponding to AD8232 chip's documentation (Figure 6), the cutoff frequency of the low-pass filter is 41.09 Hz. [11]

$$G_L = 1 + \frac{R_6}{R_7} \tag{3}$$

The resistors R_6 and R_7 presents in Figure (6) correspond to the gain and can be modified as presented in (3). Using the values $R_6 = 1M\Omega$ and $R_7 = 100K\Omega$, the gain of this stage is 11.

3) Band-Pass Filter: The analog filter behavior is shown in Figure 5. c). furthermore, the AD8232 provides an additional resistor R_{comp} that can be used to control the quality Factor (Q) of the filter to achieve narrow band-pass filters. Equation (4) presents the R_{comp} calculation.

$$R_{comp} = 0.14R_1 \tag{4}$$

The quality factor of the band-pass filter requires a value greater than 0.7 for maximum flatness and sharp cut-off according to AD8232 datasheet [11]. Equation (5) corresponds to the quality factor value.

$$Q = \frac{\sqrt{R_4 C_4 R_5 C_5}}{R_5 C_4 + R_4 C_4 + R_5 C_5 (1 - G)} \tag{5}$$

By applying the values presented in Figure 6 the quality factor value is $Q = 0.775$. At the same time, the band-pass filter gain is $G_B = 1100$. The manufacturer provides software called AD8232 Filter Design that was used in this study to validate the correct behavior of the analog stage designed. Figure 7 shows the band-pass filter designed.

At the same time, Figure 8 shows the Analog Stage filter in dB, this graphic allows validating the correct design of the analog filters.

Equation (6) presents the Gain in dB, where G corresponds to the function's gain in (V/V).

$$G_{dB} = 20 \log G \tag{6}$$

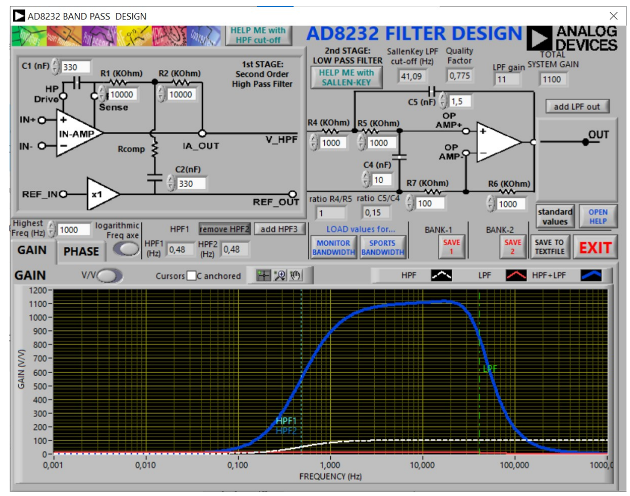

Fig. 7. EOG circuit and V/V response using Filter Design software. Blue graphic: Band-pass filter behavior in the frequency range. [13], Copyright © 2019, Analog Devices, Inc. All Rights Reserved.

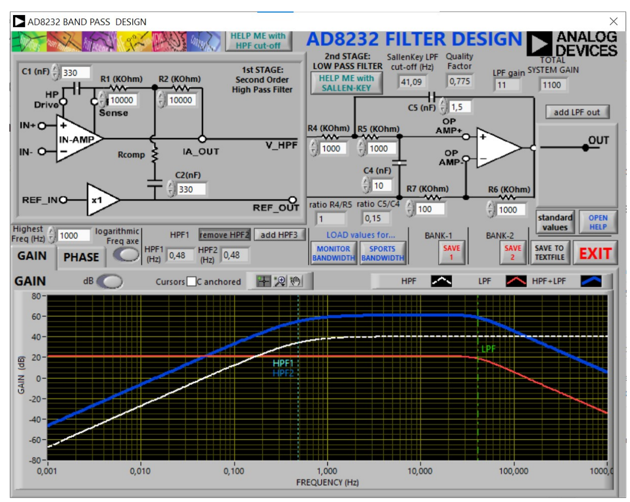

Fig. 8. EOG circuit and response in dB using Filter Design software. Low-Pass Filter (Red), High-Pass Filter (White), and by integrating, the Band-Pass Filter (Blue) response. [13], Copyright © 2019, Analog Devices, Inc. All Rights Reserved

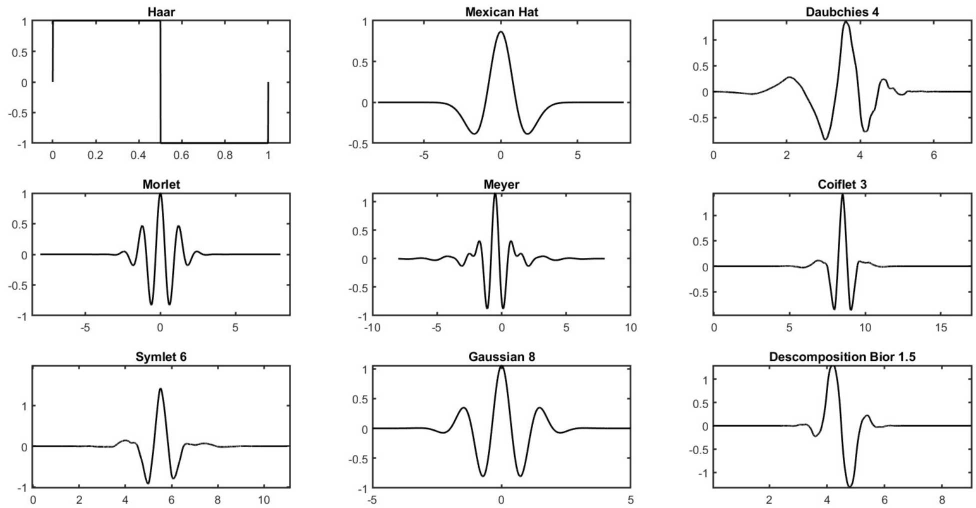

Fig. 9. Different Wavelet Functions Families.

C. System on a chip - SOC

To establish the SOC used in this study, different alternatives were compared as is presented in table II. Due to the Bluetooth and WiFi communication protocols, and its double core, the ESP32-WROOM-32D is the selected device. [14]

TABLE II
SOC COMPARISON

Specifications	ESP32	STM32F469	ATmega328P
SRAM [KB]	520	384	2
Frequency [MHz]	240	180	20
Flash [KB]	4	2000	32
Cores	2	1	1
Communication Protocols	BT[3]/WiFi I2C/SPI/ UART/Ethernet	Ethernet UART/I2C/ USART	USART SPI/I2C
Documentation	Good	Regular	Excellent

D. ADC and communication subsystems

The ADS1115 device is in charge of digitizing the EOG signals to be acquired by the SOC. This device was rated frequency of 860 SPS, satisfying the Nyquist frequency (7).

$$N_f \geq 2 \cdot F_{max} \quad (7)$$

Besides, according to the maximum voltage measured through an oscilloscope at the output of the AFEs, a suitable value to avoid signal saturation is the 1.024v full scall range setting. [15]

For the communication subsystem it was made a comparison table III between different possible communication methods between the SOC and the PC like Zigbee, Bluetooth, and UART. [16] [17] [18]

According to the table III and the characteristics of ESP32-WROOM-32D, Bluetooth was implemented as the wireless communication protocol and UART as the wired communication protocol, requiring a USB converter device. In this case, the CP2102. [19]

[3]Bluetooth

TABLE III
COMMUNICATION PROTOCOLS

Specifications	Bluetooth 4.2[4]	Zigbee 3.0	UART
Voltage supply [v]	1.8-3.9	2.1-3.6	1.8-3.9
Current Input [A]	0.5[5]	0.04	0.5
Range [m]	30[6]	60	15(cable)
Data Rate[Mbps]	1.0	0.25	5.0

E. Digital filtering process

In Analog electrical signals filtering the interference signals delete does not occur entirely or in some cases appear another interference signal (60 Hz) as a result of the electrical network. The Wavelet Transform method was chosen for digital processing, due to its viability for the treatment of non-stationary signals as EOG signal, furthermore its versatility, and analysis in the frequency and temporal spectra. [21].

F. Wavelet transform

Wavelet transform consists of decomposing a signal into scaled and shifted versions of the main signal. Equation (8) presented the Wavelet Transform Definition. [22]

$$W_f(s,\tau) = \int f(t)\psi_{s,\tau}(t)dt \quad (8)$$

Wavelets act as bandpass filters and can be of two different relationships, such as temporal-frequency or temporal-scalar

[4]Integrated to ESP32-WROOM-32D
[5]Minimum current for ESP32-WROOM-32D
[6]According to "The Bluetooth range estimator" and ESP32-WROOM-32D datasheet [20]

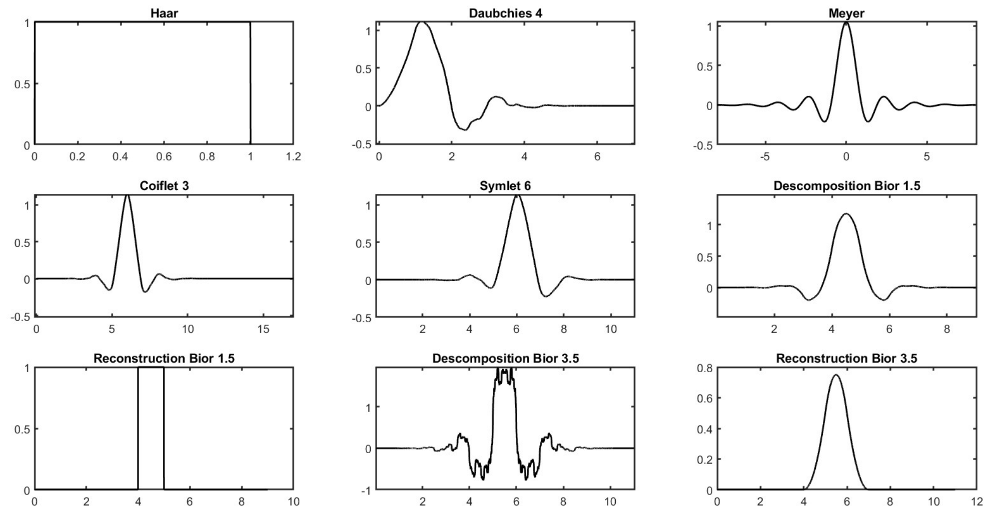

Fig. 10. Different Scale Functions Of Wavelet Families.

depending on the signal to be analyzed. A wavelet signal is defined as an equation (9)

$$\psi_{s,\tau}(t) = \frac{1}{\sqrt{s}}\psi\left(\frac{t-\tau}{s}\right);\ s,\tau \in \mathbf{R}, s \neq 0 \tag{9}$$

ψ is the base function of the analysis signal, considering the scale parameters s and translation parameters τ implemented in order to expand or contract the signal or to make temporary movements of the signal respectively. [10], [22].

The wavelet transforms comprise the continuous wavelet transform (CWT) and the discrete wavelet transform (DWT) applied in this study. Besides, is important the correct selection of the wavelet functions classified in different families according to similar characteristics between them. Figure 9 presents different wavelet families.

1) Discrete wavelet transform: The DWT consists of the application of the WT with a digitized signal, acquiring the frequency and time information of the signal. Some of the wavelet functions that can be applied to DWT are the Haar, Symlet, Daubechies, Coiflets, and Biorthogonal wavelet families. DWT is defined as:

$$DWT_{\psi}(i,k) = \int_{-\infty}^{\infty} f(t)\psi_{i,k}(t)dt;\ i,k \in \mathbf{Z} \tag{10}$$

Where variables i,k are integers values that scale or dilate the base wavelet and $\psi(t), \phi(t)$ represent the associated wavelet and scale functions shown in (11) and (12).

$$\psi_{i,k}(t) = s_o^{\frac{-i}{2}} \cdot \psi(s_o^{-i}t - k\tau_o);\ i,k \in \mathbf{Z}, s_o = 2,\ \tau_o = 1 \tag{11}$$

$$\phi_{i,k}(t) = s_o^{\frac{-i}{2}} \cdot \phi(s_o^{-i}t - k\tau_o);\ i,k \in \mathbf{Z}, s_o = 2,\ \tau_o = 1 \tag{12}$$

Besides, it is important to know that the biorthogonal wavelets have two-scale and wavelet functions, where each pair is used for decomposition or reconstruction. Figure 10 presents different scale wavelet function and both, decomposition and reconstruction biorthogonal scale function.

The approximations made with the help of the scale function allow a multi-resolution analysis that consists of analyzing the signal of interest in multiple frequency bands establishing a concatenation of subspaces where all the information of the resolution level i is contained in the resolution level $(i-1)$ as shown in (13). [23]

$$\xi_{i,0} \subset \xi_{i-1,0} \subset \ldots \subset \xi_{1,0} \subset \xi_{0,0} \tag{13}$$

Based on this, the original function $f(t)$ can be approximated by the synthesis equation (14). [24]

$$f(t) = \sum_k \sum_i C_{i,k} \cdot \phi_{i,k}(t) + \sum_k \sum_i D_{i,k} \cdot \psi_{i,k}(t);\ i,k \in \mathbf{Z} \tag{14}$$

In equation (14) the terms $C_{i,k}$ and $D_{i,k}$ correspond to the coefficients of scale or of approximation and wavelet or detail coefficients, respectively [10], [24]. Equation (15) and (16) presents the approximation and details coefficients.

$$C_i[n] = \int_{-\infty}^{\infty} f(t) \cdot \phi_{i,k}(t)dt \tag{15}$$

$$D_i[n] = \int_{-\infty}^{\infty} f(t) \cdot \psi_{i,k}(t)dt \tag{16}$$

Through the sequence of wavelet coefficients, a general study of the signal $f[n]$ can be represented.

$$F = \{D_1[n], D_2[n], \ldots, D_i[n], C_i[n]\} \tag{17}$$

From the equation (17) it follows that when a signal is decomposed at a level i, we obtain i coefficients of detail and a coefficient i_{esimo} of approximation. These C and D coefficients can be calculated through the recursive downsampling and

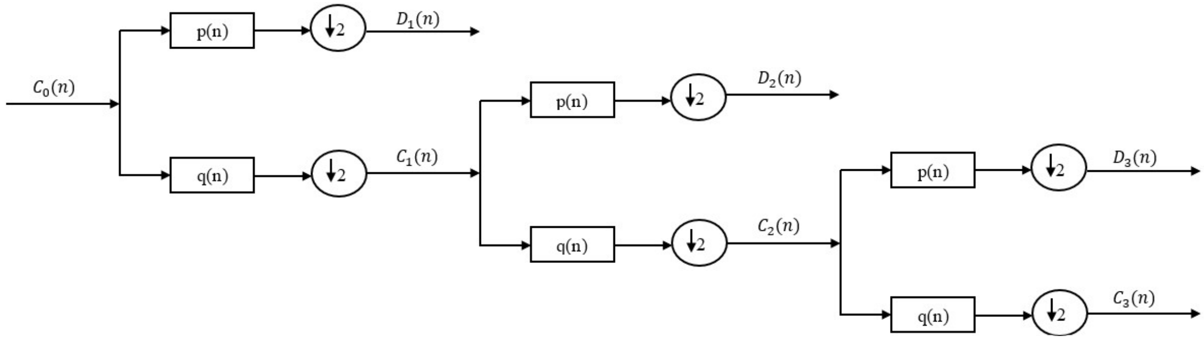

Fig. 11. Wavelet series decomposition scheme in level ($i = 3$). D: Details coefficients. C: Approximation coefficients. p(n): High pass filter decomposition wavelet q(n): Low pass filter decomposition wavelet.

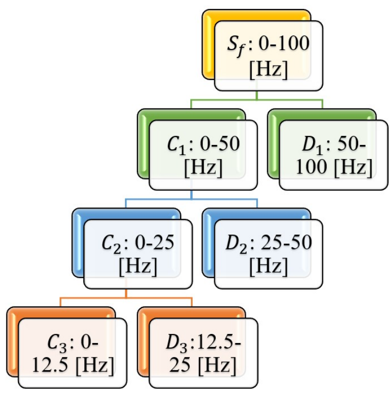

Fig. 12. Mallat algorithm decomposition for 100 Hz. Yellow (S_f): Original signals frequency. Green (C_1, D_1): First decomposition level frequencies. Blue (C_2, D_2): Second decomposition level frequencies. Red (C_3, D_3): Third decomposition level frequencies.

upsampling filters respectively. This algorithm is known as the Mallat algorithm shown in Figure 11.

Once you have the discrete wavelet transform and the characteristics of the EOG signals, the digital processing process can be carried out to reduce the interference signals. Figure 13 shows a general scheme of the discrete wavelet transform denoising.

Fig. 13. General Scheme Of Digital Processing.

It is essential to take into account that for each level of decomposition the frequency decreases at half intervals from the original frequency of the signal of interest (see Figure 12). Is due to this and the number of signal samples that the decomposition of a signal input can be performed up to a decomposition level $Nivel = \log_2(N)$, where N corresponds to the number of samples of the signal of interest.

2) Threshold techniques: Digital filtering through DWT requires a threshold value of λ to be set. This threshold technique is based on a numerical value to establish the values, at each level of wavelet decomposition, that corresponds to the interference signal. The threshold value can be a universal or recursive value where the universal threshold corresponds to a value to apply to all coefficients of the signal to be processed and the recursive threshold value is established for each level of decomposition, having n threshold values (λ), where n corresponds to the level of decomposition. For the calculation of the threshold, the following statistical parameters were considered.

- VisuShrink: This is an extension of the "Universal" statistical threshold, in which a weighting is performed between this statistical threshold and the standard deviation of the samples at each wavelet decomposition level. [25]

$$\lambda = \sigma^2 \sqrt{2\log(N)} \tag{18}$$

  Where N represents the number of samples and σ is the standard deviation value calculated with the mean absolute deviation of the wavelet coefficients of the processed signal.

$$\sigma = \frac{MAD(|coefficients|)}{0.6745} \tag{19}$$

- BayesShrink: The goal of the BayesShrink method is to minimize the risk. This method uses soft thresholds and depends on the level of resolution in the wavelet decomposition. which was claimed to often provide a better denoising result than the SURE threshold. [26]

$$\lambda = \frac{\sigma^2}{\sigma_s^2} \tag{20}$$

  Where σ^2 is the noise variance and the σ_s^2 is the signal variance without noise.

Also, the selection of the digital filtering method is related to the interference signal elimination methodology based on the established threshold values. Some methods of denoising in digital filtering are "Hard", "Soft" and "Garrote" shrinkage.

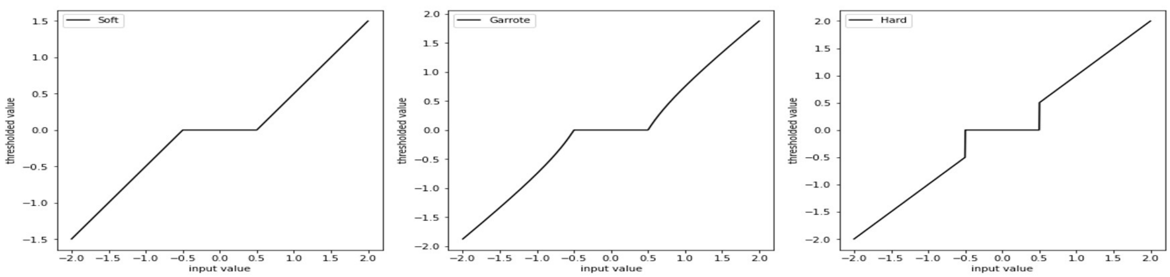

Fig. 14. Contraction Method. Soft Shrinkage. Garrote Shrinkage. Hard Shrinkage

- Hard shrinkage: Consists of maintaining the value of the analyzed detail coefficient if its absolute value is greater than the calculated threshold value or established a zero value if is lower. [24]

$$CDN_{i,j} = \begin{cases} 0, & |CD_{i,j}| < thr \\ CD_{i,j}, & |CD_{i,j}| \geq thr \end{cases} \tag{21}$$

- Soft shrinkage: Maintains the value of the detail coefficient if its absolute value is greater than the value established as the threshold and if it is lower than the estimated threshold value a linearization is performed as is shown in (22). [24]

$$CDN_{i,j} = \begin{cases} sign(CD_{i,j})(CD_{i,j} - thr), & |CD_{i,j}| < thr \\ CD_{i,j}, & |CD_{i,j}| \geq thr \end{cases} \tag{22}$$

- Garrote shrinkage: The "garrote" shrinkage eliminates the coefficients if its absolute value is greater than the value established as the threshold and reduces large coefficients by a non-linear function if it is lower. [24]

$$CDN_{i,j} = \begin{cases} 0, & |CD_{i,j}| < thr \\ CD_{i,j}\left(1 - \left(\frac{thr}{CD_{i,j}}\right)^2\right), & |CD_{i,j}| \geq thr \end{cases} \tag{23}$$

G. Statistical parameters

This section includes four statistical parameters used for the correct selection of the denoising method .

- MSE: It is a statistical parameter, which represents the squared average errors, that is, the difference between the original signal and the filtered signal. [27]

$$MSE = \frac{1}{N}\sum_{x=1}^{N}[s(x) - s_f(x)]^2 \tag{24}$$

Where $s(x)$ represents the original EOG signal and $s_f(x)$ represents the filtering EOG signal. Besides N is the data length.

- PRD: The mean square root percentage allows obtaining the error of the original signal with the estimated signal at each of its points. Equation (25) shows the calculation of the PRD. [28]

$$PRD = \sqrt{\frac{\sum_{x=1}^{N}[s(x) - s_f(x)]^2}{\sum_{x=1}^{N}[s(x)]^2}} \tag{25}$$

- SNR: It expresses the relationship between signal strength and signal noise. This relationship is measured in dB and is calculated as. [29]

$$SNR = 10\log\left(\frac{\sum_{x=1}^{N}[s(x)]^2}{\sum_{x=1}^{N}[s(x) - s_f(x)]^2}\right) \tag{26}$$

- PSNR: It expresses the relationship between the maximum value of the signal strength and signal noise. This relationship is measured in dB and is calculated as. [27]

$$PSNR = 10\log\left(\frac{Max^2}{\sum_{x=1}^{N}[s(x) - s_f(x)]^2}\right) \tag{27}$$

Where Max represents the maximum value in the EOG signal.

H. Open source software process

Digitized data is manipulated programmatically, as an overview, first, data goes through the SOC, programmed with the open-source Arduino IDE based on C language. EOG data is acquired and transmitted through wireless communication by Bluetooth protocol to the software Spyder, which is an open-source scientific environment written in Python implementing the NumPy, serial, CSV, skimage, matplotlib, and datetime libraries. Digitally filtered, organized, saved, and plotted is realized in this software. The detailed purpose and structure of both are presented below.

1) Acquisition and digital transmission process: The Arduino code programmed in 2 independent cores of the ESP32-WROOM-32D is responsible for the Bluetooth connection, the ADC configuration, and the data transmission between the EOG device and the PC. The lack of information is avoided by a synchronized timer, taking 100 samples per second for each of both movements (horizontal and vertical). Figure 15 and 16 shows the algorithm implemented.

2) Digital filtering process: In Python code, the data is received for later digital filtering through the DWT, graphed, and digitally stored as a CSV file. The amount of data to be acquired and the location of the created CSV must be previously defined for this purpose.

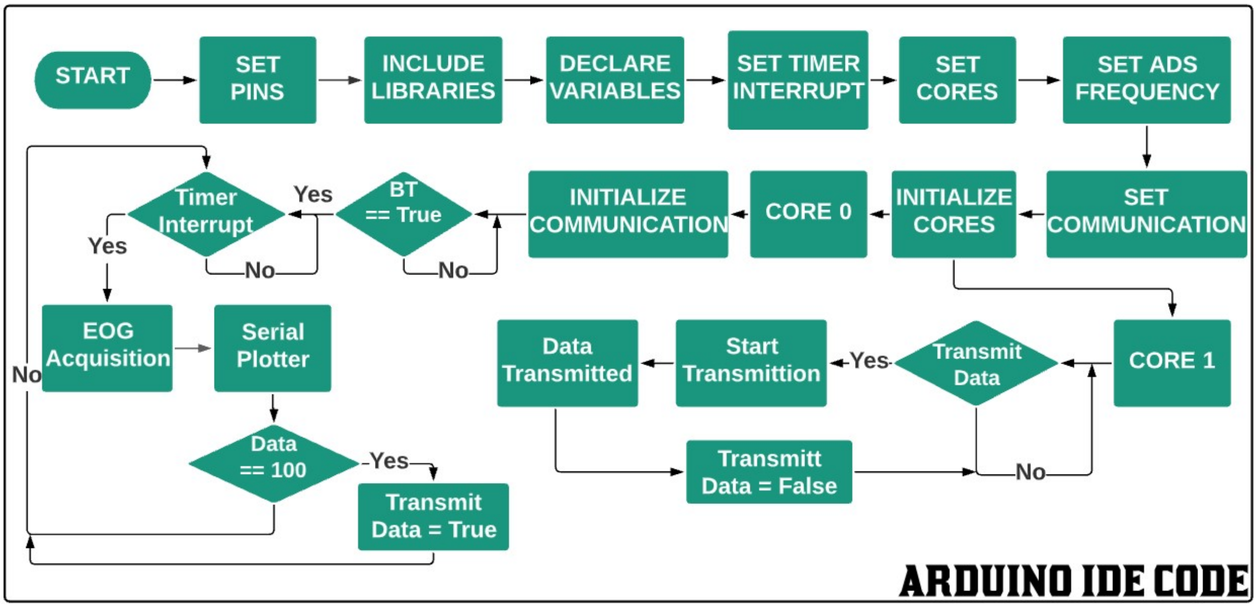

Fig. 15. Arduino IDE Code Diagram. General flow chart that indicates the processes made in both cores (BT: Bluetooth)

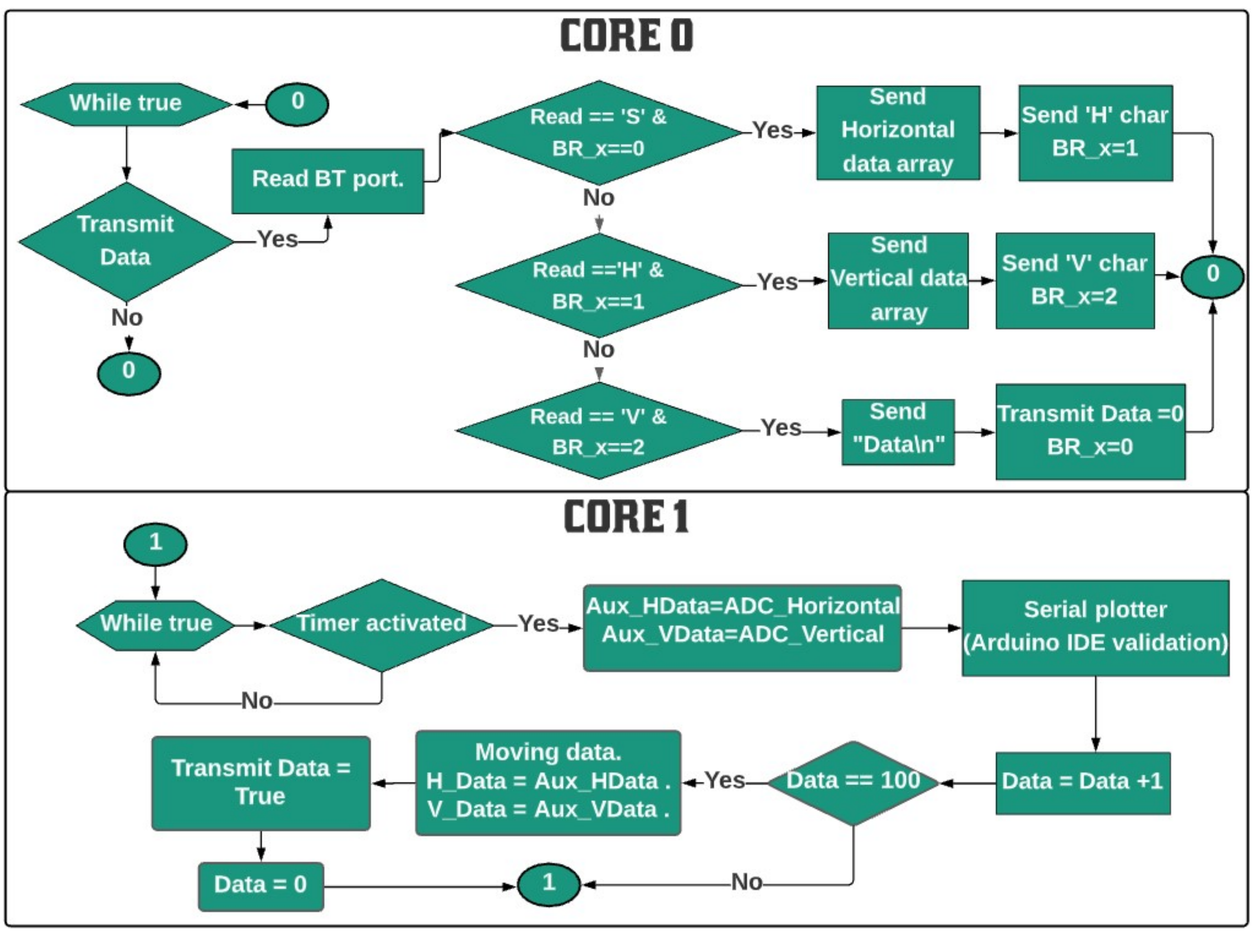

Fig. 16. Arduino IDE Cores Diagram. It shows detailed information about the processes made in each core. Core 0 sends the information via bluetooth every 1 second. Core 1 acquires the data every time that the timer is activated and save it in arrays. (BT: Bluetooth)

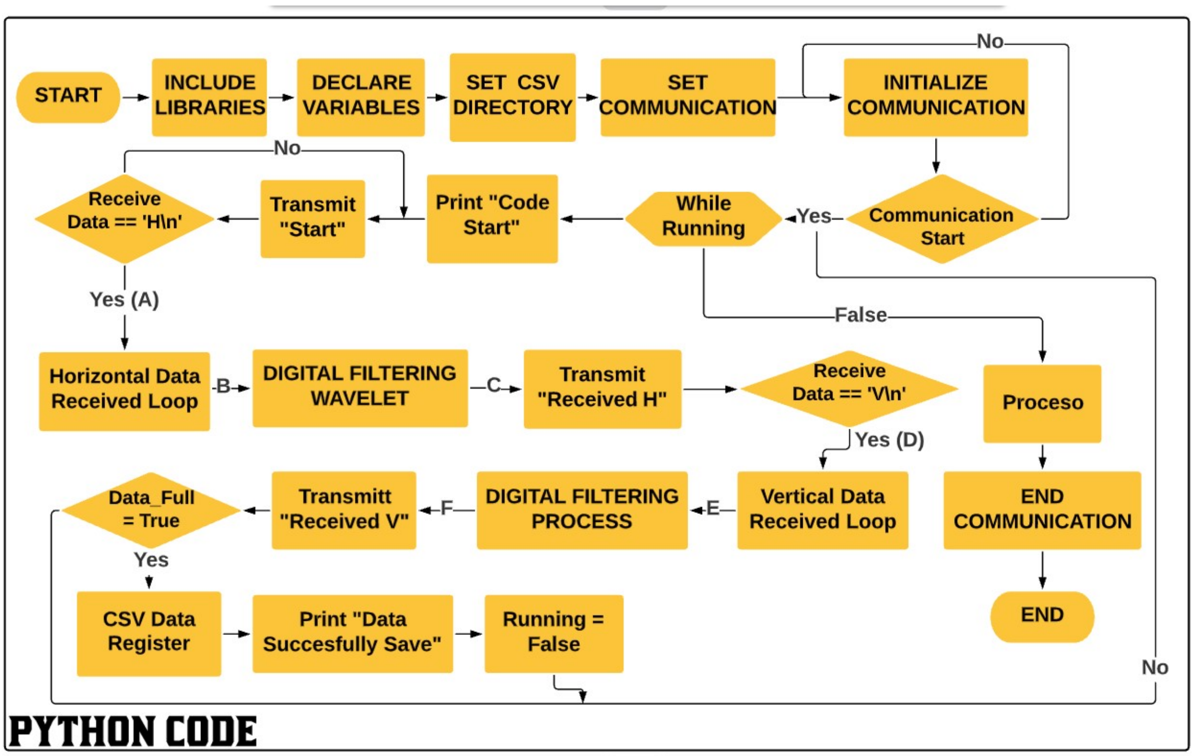

Fig. 17. Python Code. This code receives the EOG data from the PCB through Bluetooth communication and then applies the wavelet digital filter, storage this data in a csv file and then plots them.

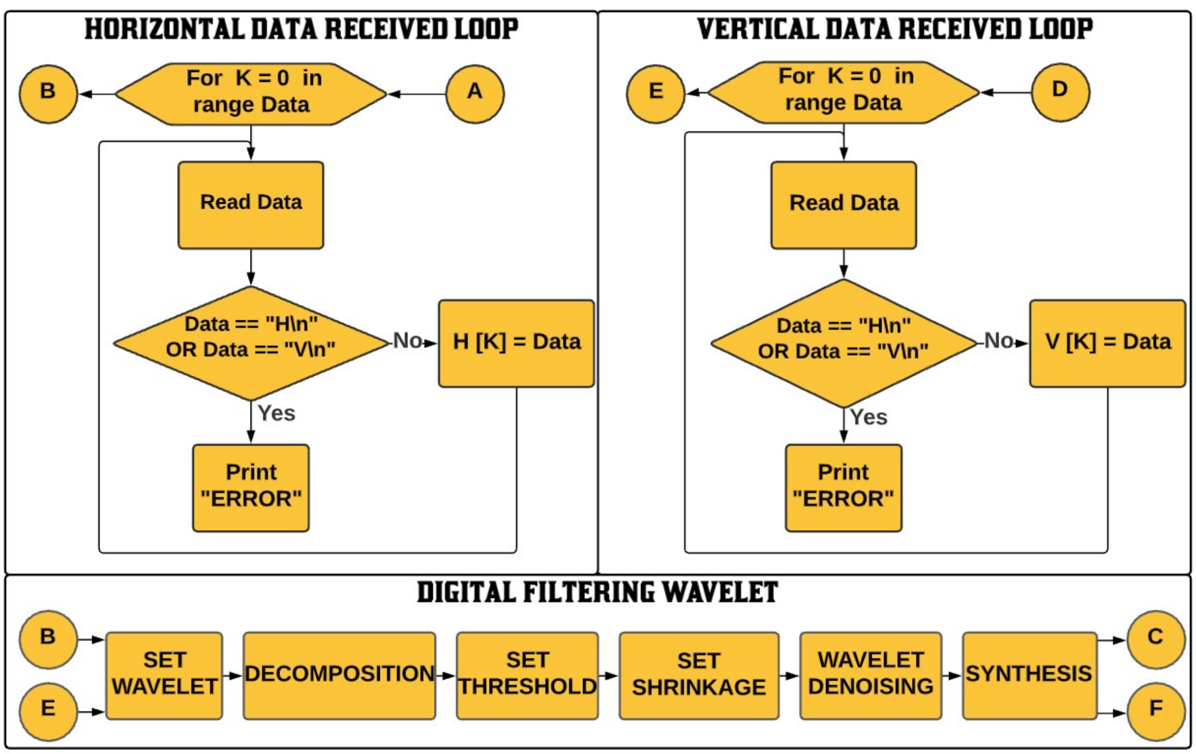

Fig. 18. Python Code Functions Diagram. Horizontal data received loop: Starts the acquisition of horizontal EOG data and stores it in the horizontal data array. Vertical data received loop: Starts the acquisition of vertical EOG data and stores it in the vertical data array. Digital filtering wavelet: It sets the wavelet digital filter configurations and then applies the filter to the acquired data.

III. Results and discussion

The subsystems of the prototype were validated individually by tests in different subjects for 16 seconds, where vertical and horizontal eye movements were validated. A correct filter step at the output of both AFEs, an accurate analog to digital data conversion, and also a correct Bluetooth communication, digital filtering, and digital data acquisition were validated. Furthermore, for the digital filter, different wavelet functions were tested to find the best result.

A. Developed device

The designed device is a PCB with dimensions of 64mm ∗ 70mm and is shown in figure 19, where different subsystems are tagged. LOD pins are the lead of detection pins from each AFE, used to test their correct configuration, and the third pin is connected to the filtered signal, which is the output signal of the AFEs.

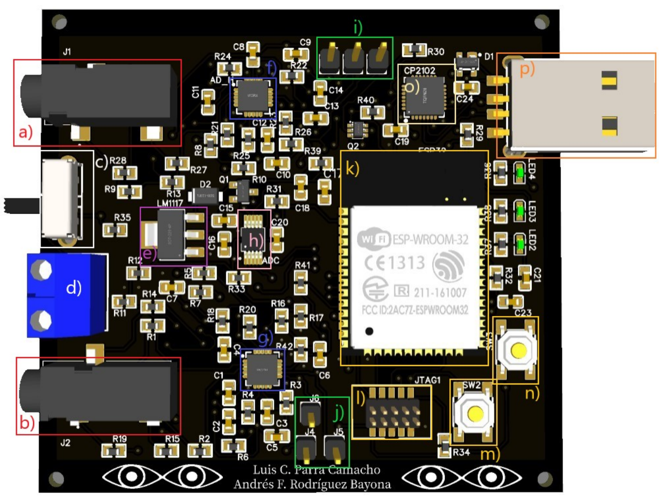

Fig. 19. Developed EOG Device. a) Horizontal signals Jack. b) Vertical signals jack. c) ON-OFF switch. d) Power input. e) Voltage regulator f) AFE for horizontal signals. g) AFE for vertical signals. h) ADC. i) LOD and AFE output pins for horizontal data. j) LOD and AFE output pins for vertical data. k) ESP-WROOM-32 SOC. l) JTAG. m) Reset button. n) Boot button. o) CP2102. p) USB pin.

The physical components for this project are shown in figure 20. These components were used for testing the device, for this testing both power inputs were used individually, so they could be validated, LOD pins were measured through an oscilloscope, showing a voltage value of 0 when the electrodes were measuring the EOG signals. The filtering stages were validated by measuring the filtered signal with an oscilloscope, presenting a signal that responds to eye movement, thus demonstrating a correct frequency range of the filters. This signal acquired is in voltage ranges from 0 to 500 mv as shown in figure 23 and 22. Also, the device was connected to a PC through USB and Bluetooth for plotting the measured signals, validating the subsystem communication. The analog and digital signals appear in the next subsection.

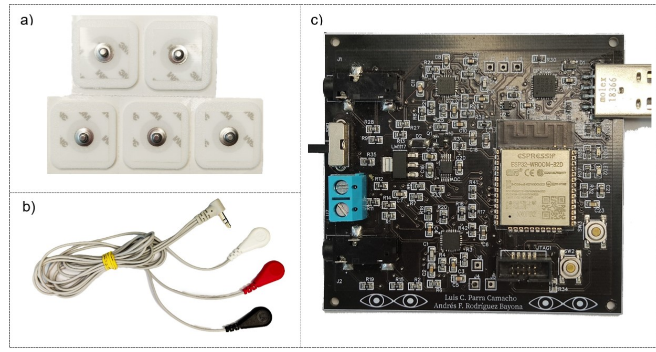

Fig. 20. EOG Device Components. a) Electrodes 3M 2228. b). ECG cable. c) Developed EOG device.

B. EOG Acquisition

Data acquired requires different subsystems to work appropriately. As was mentioned, in the way to improve the correct data acquired and transmission were implemented both cores of ESP32-WROOM-32D used in this prototype. In this way, core 0 is implemented in the transmission data and core 1 is implemented in the data acquisition according to Nyquist frequency.

The data acquired is very similar to the analog data seen from an oscilloscope. This digital data is sampled once every 10 ms for both AFEs, which means a frequency of 100Hz, being higher than the 82.18 Nyquist frequency (7). For the ADC configurations, it was found that a low sampling frequency can cause the alteration of the activation time of the timer configured in ESP32-WROOM-32D, resulting in the impossibility of reconstruction of the EOG signal.

Otherwise, a high sample rate causes higher levels of noise or interference of the desired signal, and a suitable sample value is important for this task, in Figure 21 it is displayed the original EOG signal and the EOG signal acquired at three different Nyquist frequencies, for these reasons, the ADS1115 sample rate established was 868*SPS*.

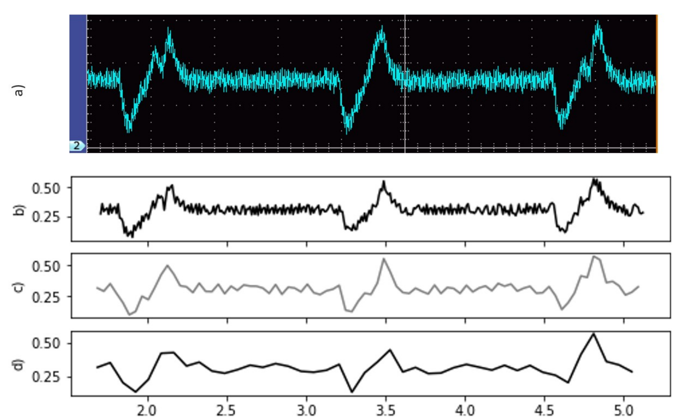

Fig. 21. Comparison of different sampling frequency. (a) Analog Signal. (b) 100Hz digital signal. (c) 25Hz digital signal. (d) 12.5Hz digital signal.

Based on this, the acquisition of the horizontal and vertical EOG signal was performed with the valid Nyquist frequency using the software Arduino IDE for the serial protocol and the Python development environment for the Bluetooth protocol. These signals were compared with the signal obtained through the oscilloscope. Figure 22 shows the horizontal EOG signal acquired. Also, Figure 23 shows the vertical EOG signal acquired.

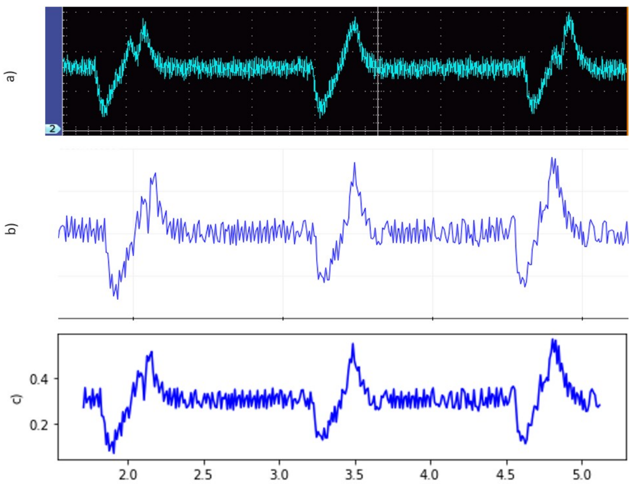

Fig. 22. Horizontal EOG Signal Acquired. (a) Analog signal measured from the oscilloscope. (b) Digital signal acquired through serial protocol. (c) Digital signal acquired through Bluetooth protocol

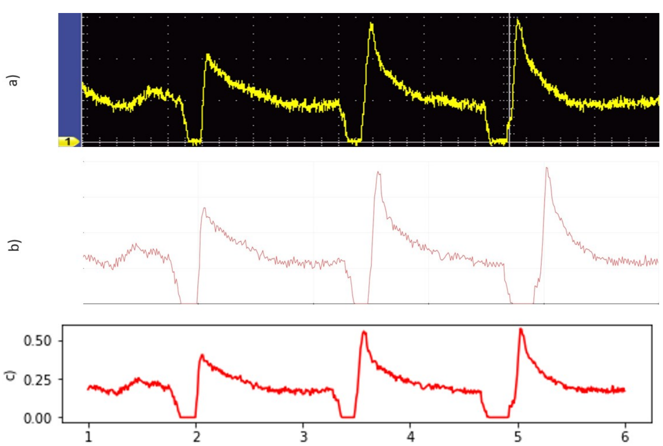

Fig. 23. Vertical EOG Signal Acquired. (a) Analog signal measured from the oscilloscope. (b) Digital signal acquired through serial protocol. (c) Digital signal acquired through Bluetooth protocol

Furthermore, the vertical EOG signal captures the electrical variations present by both voluntary and involuntary blinks. On the other hand, the horizontal signal does not present electric potential before the flickers. Figure 24 shows the flickers presented in the vertical EOG signal.

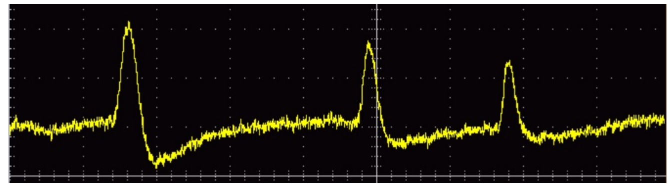

Fig. 24. Influence of flickers on the vertical EOG signal.

C. EOG Denoising

The data obtained for both the vertical and horizontal movements of the eye were implemented to establish which wavelet function is more optimal in the digital processing explained above. The Python Spyder software was used to carry out this task. To establish the most suitable wavelet for processing, 4 wavelet families were analyzed (Haar, Symlet, Coiflet, and Daubechies). Besides, the different thresholds explained were analyzed to the correct selection of denoising in the wavelet decomposition. Figure 25 shows a horizontal signal acquired filtering by the wavelet "Coiflet 5" and a "hard" threshold.

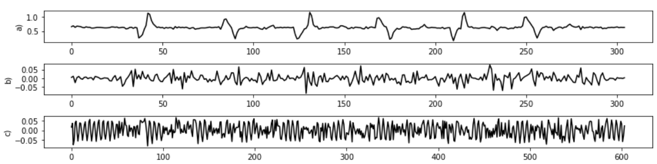

Fig. 25. Horizontal EOG Wavelet Decomposition

The individual analysis of each one of the statistical parameters calculated can generate erroneous conclusions, being necessary an analysis in the set of the information for a suitable selection, these parameters of wavelet functions applied in digital filter for EOG signals can be useful in future projects about EOG signal processing. . Tables IV and V show the calculated values for the average of three different registers of horizontal and vertical signals respectively. Taking into account that the MSE and PRD values must be low and the statistical parameters SNR and PSNR high, the analysis of the information presented was carried out. In the horizontal signal, table IV shows that the best wavelet was the Coiflet 5. However, all results were the same, regardless of the filtering method or threshold type. Due to this, and based on the other information in the table, it was observed that the BayesShrink method has better results compared to the VisuShrink. Furthermore, the hard threshold was the best. Figure 26 shows horizontal signal with the denoising process established. Likewise, the analysis was performed for the vertical signals. Table V shows the results obtaining the best for the wavelet "coif4" with a "BayesShrink" threshold and a "hard" contraction. Figure 27 shows vertical signal with the denoising process established. As can be seen in figures 26 and 27 the signal reconstructed also horizontal as vertical shows the correct denoising process avoiding delete important information of the EOG signal.

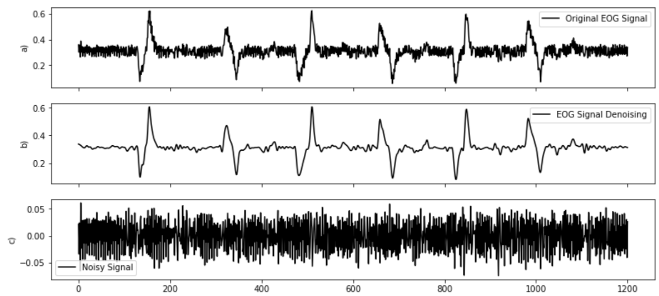

Fig. 26. Horizontal EOG Wavelet Denoising through "Coif5", "BayesShrink" threshold and "Hard" contraction. a) Original Signal. b) Denoised Signal. c) Noisy.

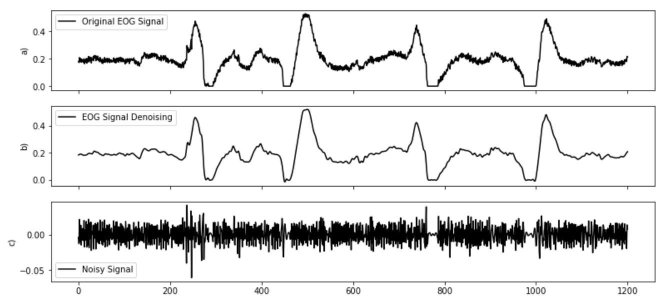

Fig. 27. Vertical EOG Wavelet Denoising through "Coif4", "BayesShrink" threshold and "Hard" contraction. a) Original Signal. b) Denoised Signal. c) Noisy.

D. Eye movement characterization

Input	Horizontal signal	Vertical signal	Output
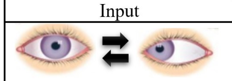	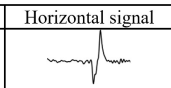	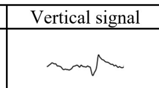	Left
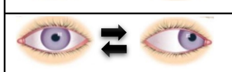		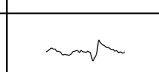	Right
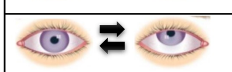	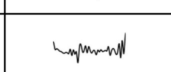	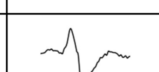	Up
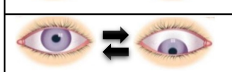	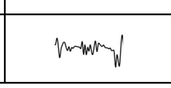	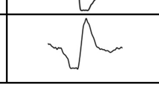	Down

Fig. 28. EOG Signal Characterization.

The EOG signal amplitude is affected when is tested on different subjects and at the same time, it is affected by the speed of eye movement. This can be considered a limitation of the study presented, nonetheless, the characterization and the waveform acquired are not highly altered by this. The characterization of the signals acquired and processed through the different analog and digital stages of the developed prototype are shown in Figure 28, evidencing an average behavior of the signals for each eye movement evaluated, allowing their characterization. Finally, it must be said that this project can serve as a starting point for future projects, such as characterizing the EOG signals through computer science applications or the development of applications where the EOG signals may be studied or used, like, the study of polysomnography or the control of a wheelchair through eye movements.

TABLE IV
DIFFERENT WAVELET ANALYSIS IN HORIZONTAL EOG SIGNAL

	Wavelet	Threshold	Shrinkage	MSE	PRD	SNR(dB)	PSNR(dB)
Haar	**Haar** 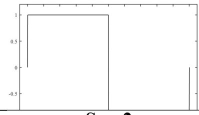	VisuShrink	Hard	0.001564207	0.124955853	18.09509203	22.53823655
			Garrote	0.001799290	0.134079365	17.47502770	21.91817222
			Soft	0.002045495	0.142935241	16.91626211	21.35940663
		BayesShrink	Hard	0.001177698	0.108193597	19.37193451	23.81507902
			Garrote	0.001193619	0.108925478	19.31270238	23.75584690
			Soft	0.001226971	0.110460366	19.18830569	23.63145021
Symlet	**Sym2** 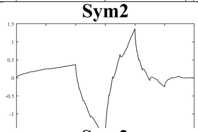	VisuShrink	Hard	0.001358810	0.116505231	18.69981488	23.14295940
			Garrote	0.001484705	0.121793973	18.30933652	22.75248104
			Soft	0.001633707	0.127652697	17.90475283	22.34789735
		BayesShrink	Hard	0.001155955	0.107398753	19.41489391	23.85803843
			Garrote	0.001176340	0.108362814	19.33477988	23.77792439
			Soft	0.001206322	0.109752860	19.22185562	23.66500014
	Sym3 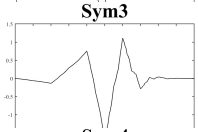	VisuShrink	Hard	0.001266721	0.112523805	18.99541224	23.43855676
			Garrote	0.001335779	0.115531863	18.76442690	23.20757142
			Soft	0.001392310	0.117895859	18.58907434	23.03221886
		BayesShrink	Hard	0.001136815	0.106286146	19.52763118	23.97077570
			Garrote	0.001161165	0.107452037	19.42868648	23.87183100
			Soft	0.001188084	0.108750196	19.31753777	23.76068229
	Sym4 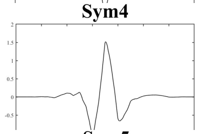	VisuShrink	Hard	0.001234457	0.111002177	19.12330335	23.56644787
			Garrote	0.001309891	0.114437479	18.84551122	23.28865574
			Soft	0.001365757	0.116815205	18.66612296	23.10926748
		BayesShrink	Hard	0.001139234	0.106272041	19.54171103	23.98485555
			Garrote	0.001154834	0.107031598	19.47582362	23.91896814
			Soft	0.001176639	0.108112187	19.38036904	23.82351356
	Sym5 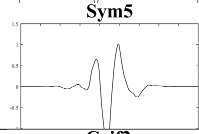	VisuShrink	Hard	0.001228160	0.110679090	19.15276659	23.59591111
			Garrote	0.001274699	0.112854068	18.97224106	23.41538558
			Soft	0.001325045	0.115078000	18.79827871	23.24142323
		BayesShrink	Hard	0.001149158	0.107131997	19.43058288	23.87372740
			Garrote	0.001160136	0.107614823	19.39417621	23.83732073
			Soft	0.001174335	0.108250562	19.34477582	23.78792034
Coiflet	**Coif2** 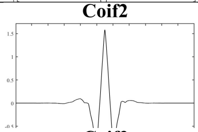	VisuShrink	Hard	0.001128451	0.106183220	19.50403476	23.94717928
			Garrote	0.001136022	0.106560993	19.47051145	23.91365597
			Soft	0.001141648	0.106838896	19.44609611	23.88924063
		BayesShrink	Hard	0.001077700	0.103527475	19.75134026	24.19448478
			Garrote	0.001089788	0.104181071	19.68848900	24.13163352
			Soft	0.001103150	0.104887566	19.62205101	24.06519553
	Coif3 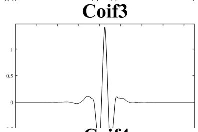	VisuShrink	Hard	0.001097478	0.104688715	19.63098352	24.07412803
			Garrote	0.001111206	0.105390215	19.56723226	24.01037678
			Soft	0.001116855	0.105674444	19.54179631	23.98494083
		BayesShrink	Hard	0.001072858	0.103389953	19.75285115	24.19599567
			Garrote	0.001086279	0.104104707	19.68514932	24.12829384
			Soft	0.001097004	0.104664228	19.63323434	24.07637885
	Coif4 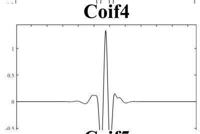	VisuShrink	Hard	0.000947881	0.097214776	20.28443639	24.72758091
			Garrote	0.000947881	0.097214776	20.28443639	24.72758091
			Soft	0.000947881	0.097214776	20.28443639	24.72758091
		BayesShrink	Hard	0.000947881	0.097214776	20.28443639	24.72758091
			Garrote	0.000947881	0.097214776	20.28443639	24.72758091
			Soft	0.000947881	0.097214776	20.28443639	24.72758091
	Coif5 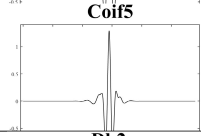	VisuShrink	Hard	0.000947532	0.097198483	20.28567115	24.72881567
			Garrote	0.000947532	0.097198483	20.28567115	24.72881567
			Soft	0.000947532	0.097198483	20.28567115	24.72881567
		BayesShrink	Hard	0.000947532	0.097198483	20.28567115	24.72881567
			Garrote	0.000947532	0.097198483	20.28567115	24.72881567
			Soft	0.000947532	0.097198483	20.28567115	24.72881567
Daubchies	**Db2** 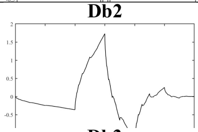	VisuShrink	Hard	0.001358810	0.116505231	18.69981488	23.14295940
			Garrote	0.001484705	0.121793973	18.30933652	22.75248104
			Soft	0.001633707	0.127652697	17.90475283	22.34789735
		BayesShrink	Hard	0.001155955	0.107398753	19.41489391	23.85803843
			Garrote	0.001176340	0.108362814	19.33477988	23.77792439
			Soft	0.001206322	0.109752860	19.22185562	23.66500014
	Db3 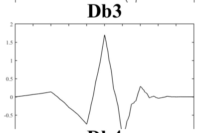	VisuShrink	Hard	0.001266721	0.112523805	18.99541224	23.43855676
			Garrote	0.001335779	0.115531863	18.76442690	23.20757142
			Soft	0.001392310	0.117895859	18.58907434	23.03221886
		BayesShrink	Hard	0.001136815	0.106286146	19.52763118	23.97077570
			Garrote	0.001161165	0.107452037	19.42868648	23.87183100
			Soft	0.001188084	0.108750196	19.31753777	23.76068229
	Db4 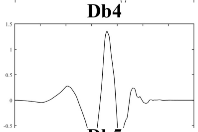	VisuShrink	Hard	0.001228189	0.110748404	19.14084974	23.58399426
			Garrote	0.001289773	0.113569764	18.91168672	23.35483124
			Soft	0.001329085	0.115289568	18.77817778	23.22132230
		BayesShrink	Hard	0.001176308	0.108147922	19.37278821	23.81593273
			Garrote	0.001196965	0.109111964	19.29316456	23.73630908
			Soft	0.001208895	0.109700979	19.24142684	23.68457136
	Db5 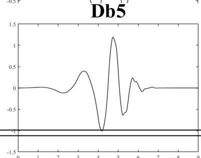	VisuShrink	Hard	0.001266040	0.112349291	19.02353336	23.46667787
			Garrote	0.001314641	0.114541250	18.84836668	23.29151120
			Soft	0.001353203	0.116237274	18.71578095	23.15892547
		BayesShrink	Hard	0.001104784	0.104711360	19.66521826	24.10836277
			Garrote	0.001126188	0.105748554	19.57610929	24.01925381
			Soft	0.001155326	0.107174405	19.45210781	23.89525233

TABLE V
DIFFERENT WAVELET ANALYSIS IN VERTICAL EOG SIGNAL

	Wavelet	Threshold	Shrinkage	MSE	PRD	SNR(dB)	PSNR(dB)
	Haar		Hard	0.000311952	0.078603002	22.09292084	30.10579409
	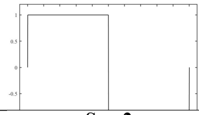	VisuShrink	Garrote	0.000422023	0.091376012	20.79096441	28.80383766
Haar			Soft	0.000675964	0.115545971	18.75526084	26.76813409
			Hard	0.000135101	0.051740085	25.76922389	33.78209714
		BayesShrink	Garrote	0.000151592	0.054838745	25.25544301	33.26831625
			Soft	0.000168121	0.057770282	24.79458794	32.80746118
	Sym2		Hard	0.000232147	0.067937897	23.36977990	31.38265315
	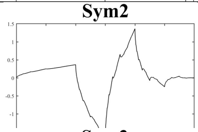	VisuShrink	Garrote	0.000292347	0.076161509	22.37411229	30.38698554
			Soft	0.000426789	0.091958569	20.73112113	28.74399438
			Hard	0.000152746	0.055099326	25.18697713	33.19985038
		BayesShrink	Garrote	0.000160562	0.056481044	24.96950492	32.98237817
			Soft	0.000168583	0.057871690	24.75722839	32.77010163
	Sym3		Hard	0.000198273	0.062803459	24.05462032	32.06749356
	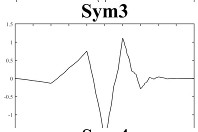	VisuShrink	Garrote	0.000244259	0.069657595	23.14327132	31.15614457
			Soft	0.000303982	0.077468022	22.22456307	30.23743631
			Hard	0.000144901	0.053657127	25.43316499	33.44603824
		BayesShrink	Garrote	0.000149367	0.054493203	25.29628893	33.30916217
Symlet			Soft	0.000155665	0.055637671	25.11519735	33.12807060
	Sym4		Hard	0.000199575	0.062969195	24.02013168	32.03300493
	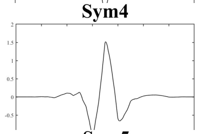	VisuShrink	Garrote	0.000239453	0.068871783	23.24080801	31.25368125
			Soft	0.000291823	0.075770793	22.42272875	30.43560200
			Hard	0.000138291	0.052429759	25.64337743	33.65625068
		BayesShrink	Garrote	0.000143614	0.053431214	25.47856337	33.49143661
			Soft	0.000151348	0.054859301	25.24512821	33.25800145
	Sym5		Hard	0.000206237	0.064036598	23.87928119	31.89215443
	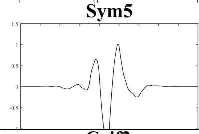	VisuShrink	Garrote	0.000236874	0.068573857	23.27930379	31.29217704
			Soft	0.000288359	0.075529023	22.44066081	30.45353406
			Hard	0.000143156	0.053317995	25.48634214	33.49921539
		BayesShrink	Garrote	0.000148163	0.054255789	25.33108841	33.34396166
			Soft	0.000155336	0.055558256	25.12315101	33.13602426
	Coif2		Hard	0.000172677	0.058572460	24.65089298	32.66376623
	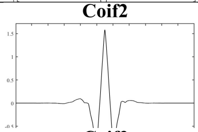	VisuShrink	Garrote	0.000190589	0.061477104	24.22837563	32.24124887
			Soft	0.000211699	0.064667153	23.79131572	31.80418897
			Hard	0.000136091	0.051997799	25.72205555	33.73492879
		BayesShrink	Garrote	0.000141724	0.053068829	25.54230402	33.55517726
			Soft	0.000148450	0.054325511	25.33310746	33.34598070
	Coif3		Hard	0.000172694	0.058506162	24.66482482	32.67769807
	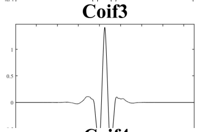	VisuShrink	Garrote	0.000190681	0.061459200	24.23149830	32.24437155
			Soft	0.000206324	0.063878957	23.89617813	31.90905138
			Hard	0.000132980	0.051414316	25.81281072	33.82568397
		BayesShrink	Garrote	0.000138578	0.052492405	25.62809033	33.64096358
			Soft	0.000145512	0.053796714	25.40956594	33.42243919
Coiflet	**Coif4**		Hard	0.000134794	0.051737512	25.73839784	33.75127108
	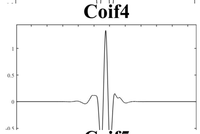	VisuShrink	Garrote	0.000139187	0.052592000	25.59049405	33.60336730
			Soft	0.000142480	0.053207171	25.48703896	33.49991221
			Hard	0.000131096	0.051067790	25.85806985	33.87094310
		BayesShrink	Garrote	0.000135281	0.051875894	25.71501539	33.72788863
			Soft	0.000138365	0.052459247	25.61407822	33.62695146
	Coif5		Hard	0.000133781	0.051537836	25.77377697	33.78665022
	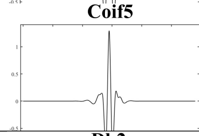	VisuShrink	Garrote	0.000138902	0.052539057	25.59912313	33.61199638
			Soft	0.000142124	0.053141467	25.49777137	33.51064462
			Hard	0.000133232	0.051482505	25.78373985	33.79661310
		BayesShrink	Garrote	0.000137169	0.052232837	25.65277965	33.66565290
			Soft	0.000139764	0.052719233	25.56944829	33.58232153
	Db2		Hard	0.000232147	0.067937897	23.36977990	31.38265315
	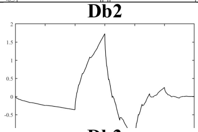	VisuShrink	Garrote	0.000292347	0.076161509	22.37411229	30.38698554
			Soft	0.000426789	0.091958569	20.73112113	28.74399438
			Hard	0.000152746	0.055099326	25.18697713	33.19985038
		BayesShrink	Garrote	0.000160562	0.056481044	24.96950492	32.98237817
			Soft	0.000168583	0.057871690	24.75722839	32.77010163
	Db3		Hard	0.000198273	0.062803459	24.05462032	32.06749356
	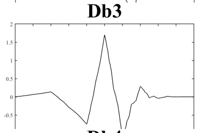	VisuShrink	Garrote	0.000244259	0.069657595	23.14327132	31.15614457
			Soft	0.000303982	0.077468022	22.22456307	30.23743631
			Hard	0.000144901	0.053657127	25.43316499	33.44603824
		BayesShrink	Garrote	0.000149367	0.054493203	25.29628893	33.30916217
Daubchies			Soft	0.000155665	0.055637671	25.11519735	33.12807060
	Db4		Hard	0.000210116	0.064559511	23.81249333	31.82536658
	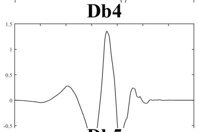	VisuShrink	Garrote	0.000249405	0.070267614	23.07377378	31.08664703
			Soft	0.000306347	0.077651727	22.21155752	30.22443076
			Hard	0.000139194	0.052621023	25.59606903	33.60894228
		BayesShrink	Garrote	0.000146534	0.053989790	25.37139747	33.38427072
			Soft	0.000153690	0.055291639	25.16384059	33.17671384
	Db5		Hard	0.000212086	0.064925698	23.76095072	31.77382396
	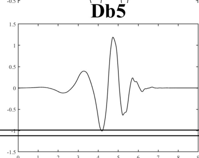	VisuShrink	Garrote	0.000250588	0.070514316	23.03655289	31.04942613
			Soft	0.000306559	0.077775085	22.18880777	30.20168102
			Hard	0.000145960	0.053846097	25.39665144	33.40952469
		BayesShrink	Garrote	0.000150451	0.054686451	25.26103120	33.27390445
			Soft	0.000156881	0.055855772	25.07648345	33.08935670

IV. CONCLUSIONS

In this project, a compact portable device able to capture EOG signals is presented. The wireless communication through Bluetooth protocol to a Spyder IDE is also presented in this work. The storage and denoises of the capture signals are developed by the PC through the Spyder software. On the other hand, the plotted signal was presented, being able to determine the direction of eye movements, such as up, down, left or right, and also blinks. The Analog front end configurations, The resolution and sampling rate of the ADC, and the SOC ESP32-WROOM-32D are important subsystems used in this work to get a high signal quality. These subsystems allow the correct filtering of the signal and are crucial to avoid a lack of information. Furthermore, the double core of the ESP32-WROOM-32D allows higher processing speeds, dividing the tasks into data acquisition and sending, and digital filtering, being crucial with integrating the other subsystems. Finally, it was verified the efficiency of different digital filter methods, among which stands out coiflet5 for horizontal signals and coiflet4 for vertical signals, both with a "BayesShrink" threshold and a "hard" contraction.

Author Contributions: Conceptualization and methodology, L.C.P, A.F.R., Hardware, L.C.P, A.F.R, D.P., Software, L.C.P, A.F.R., validation, L.C.P, A.F.R, D.P. original draft preparation, review, and editing, L.C.P, A.F.R, D.M, D.P., and final paper review, D.M, D.P. All authors have read and agreed to the published version of the manuscript.

Acknowledgment: This work has been supported and partially funded by the Santo Tomas University (Colombia).

Conflicts of Interest: The authors declare no conflict of interest.

REFERENCES

[1] World health organization, disability and health, www.who.int/news-room/fact-sheets/detail/disability-and-health#:~:text=Over%201%20billion%20people%20are,functioning%2C%20often%20requiring%20healthcare%20services, accessed: 2021-04-14.

[2] Pan American Health Organization(PAHO), www.paho.org/en/topics/disability, accessed: 2021-04-14.

[3] Article 25 – health | united nations enable, www.un.org/development/desa/disabilities/convention-on-the-rights-of-persons-with-disabilities/article-25-health.html, accessed: 2021-04-14.

[4] J. Ryu, M. Lee, D.-H. Kim, Eog-based eye tracking protocol using baseline drift removal algorithm for long-term eye movement detection, Expert Systems with Applications 131 (2019) 275–287.

[5] K. Lukander, Measuring gaze point on handheld mobile devices, in: CHI'04 Extended Abstracts on Human Factors in Computing Systems, 2004, pp. 1556–1556.

[6] P. Zhang, M. Ito, S.-i. Ito, M. Fukumi, Implementation of eog mouse using learning vector quantization and eog-feature based methods, in: 2013 IEEE Conference on Systems, Process & Control (ICSPC), IEEE, 2013, pp. 88–92.

[7] N. M. M. Noor, M. Q. bin Kamarudin, Study the different level of eye movement based on electrooculography (eog) technique, in: 2016 IEEE EMBS Conference on Biomedical Engineering and Sciences (IECBES), IEEE, 2016, pp. 792–796.

[8] R. V. G. Bermúdez, Procesamiento de registros oculares sacádicos en pacientes de ataxia sca2. aplicación del análisis de componentes independientes, Universidad de Granada (2010).

[9] M. Brown, M. Marmor, E. Zrenner, M. Brigell, M. Bach, et al., Iscev standard for clinical electro-oculography (eog) 2006, Documenta ophthalmologica 113 (3) (2006) 205–212.

[10] A. López Martínez, et al., Sistema asistencial basado en computador empleando señales electrooculográficas orientado a personas discapacitadas, Master's thesis, Universidad de Oviedo (2012).

[11] Analog Devices, Single-Lead, Heart Rate Monitor Front End.

[12] K. A. Charles, N. O. Matthew, Fundamentals of Electric Circuits, LTC, 2017.

[13] Ad8232 filter design, https://www.analog.com/en/products/ad8232.html#product-tools.

[14] Espressif, ESP32 Series Datasheet.

[15] Texas Instruments, ADS1115 Datasheet.

[16] Digi, XBee®/XBee-PRO S2C Zigbee Datsheet.

[17] O. Liberg, M. Sundberg, Y.-P. E. Wang, J. Bergman, J. Sachs, Chapter 9 - the competitive internet of things technology landscape, in: O. Liberg, M. Sundberg, Y.-P. E. Wang, J. Bergman, J. Sachs (Eds.), Cellular Internet of Things, Academic Press, 2018, pp. 327–360. doi:https://doi.org/10.1016/B978-0-12-812458-1.00009-5. URL https://www.sciencedirect.com/science/article/pii/B9780128124581000095

[18] S. Mishra, N. K. Singh, V. Rousseau, Chapter 10 - sensor interfaces, in: S. Mishra, N. K. Singh, V. Rousseau (Eds.), System on Chip Interfaces for Low Power Design, Morgan Kaufmann, 2016, pp. 331–344. doi:https://doi.org/10.1016/B978-0-12-801630-5.00010-4. URL https://www.sciencedirect.com/science/article/pii/B9780128016305000104

[19] Silicon labs, Single-chip USB to UART bridge, CP2102 datasheet.

[20] D. R. Jácome Quilumbango, Prototipo banda de muslo para la captura y acondicionamiento de las señales emg de las extremidades inferiores, B.S. thesis, Universidad Técnica del Norte (2016).

[21] J. A. C. Osorio, H. B. C. Garzón, J. A. C. Osorio, Del análisis de fourier a las wavelets-transformada continua wavelet (cwt)., Scientia et Technica 5 (37) (2007).

[22] M. Laster, Introducción a la transformada wavelet, descomposición de señales, Agencia Nacional de Promoción Científica y Tecnológica, Universidad Nacional del Centro de la Provincia de Buenas Aires (2006).

[23] L. A. Arcila Armero, L. Y. Cajas Hoyos, Análisis de señales eeg con registros de epilepsia mediante reconocimiento de patrones y transformada wavelet, Master's thesis, Universidad del Cauca (2016).

[24] H. González Acosta, Reducción de ruido digital en señales de electrocardiogramas utilizando la transformada de wavelet, Master's thesis, Universidad de Oviedo (2015).

[25] S. Sudha, G. Suresh, R. Sukanesh, Wavelet based image denoising using adaptive thresholding, in: International Conference on Computational Intelligence and Multimedia Applications (ICCIMA 2007), Vol. 3, IEEE, 2007, pp. 296–300.

[26] W. Zhang, F. Yu, H.-m. Guo, Improved adaptive wavelet threshold for image denoising, in: 2009 Chinese Control and Decision Conference, IEEE, 2009, pp. 5958–5963.

[27] A. Cedeño Pozo, R. Trujillo Codorniú, Estudio comparativo de técnicas de reducción de ruido en señales industriales mediante transformada wavelet discreta y selección adaptativa del umbral, Revista Iberoamericana de Automática e Informática industrial 10 (2) (2013) 143–148.

[28] P. Augustyniak, Adaptive sampling of the electrocardiogram based on generalized perceptual features, Sensors 20 (2) (2020) 373.

[29] I. Elyasi, S. Zarmehi, Elimination noise by adaptive wavelet threshold, World Academy of Science, Engineering and Technology 56 (2009) 462–466.